Wave runup during extreme storm conditions

Nadia Senechal,[1] Giovanni Coco,[2,3] Karin R. Bryan,[4] and Rob A. Holman[5]

Received 17 November 2010; revised 21 April 2011; accepted 12 May 2011; published 30 July 2011.

[1] Video measurements of wave runup were collected during extreme storm conditions characterized by energetic long swells (peak period of 16.4 s and offshore height up to 6.4 m) impinging on steep foreshore beach slopes (0.05–0.08). These conditions induced highly dissipative and saturated conditions over the low-sloping surf zone while the swash zone was associated with moderately reflective conditions (Iribarren parameters up to 0.87). Our data support previous observations on highly dissipative beaches showing that runup elevation (estimated from the variance of the energy spectrum) can be scaled using offshore wave height alone. The data is consistent with the hypothesis of runup saturation at low frequencies (down to 0.035 Hz) and a hyperbolic-tangent fit provides the best statistical predictor of runup elevations.

Citation: Senechal, N., G. Coco, K. R. Bryan, and R. A. Holman (2011), Wave runup during extreme storm conditions, *J. Geophys. Res.*, *116*, C07032, doi:10.1029/2010JC006819.

1. Introduction

[2] Runup is the time-varying vertical position of the water's edge on the foreshore of the beach. It is usually decomposed into a (quasi) steady component above the still water level (the wave setup) and a time-varying, fluctuating, component termed as "swash." Runup is the main driver of beachface hydro- and morphodynamics [*Elfrink and Baldock*, 2002] and so is of great relevance when studying the sediment exchanges between the subaerial and subaqueous zones of the beach [*Puleo et al.*, 2000; *Masselink and Hughes*, 1998]. Runup also plays a crtical role in dune erosion during storm conditions [*Ruggiero et al.*, 2001] and structure overtopping [*van der Meer and Stam*, 1992]. Thus, runup is key to successful coastal planning and management and a critical parameter in assessing the effect of sea level rise on coastal inundation. As one might expect, interest is primarily focused on the estimation of extreme runup during storm conditions, essential for accurate predictions of the impact on and damage to the coast.

[3] Runup characteristics change with beach and offshore wave properties. A generally accepted nondimensional parameter linking information related to beach and wave characteristics is the Iribarren number [*Battjes*, 1974], which is defined as

$$\xi_0 = \frac{\tan\beta}{(H_0/L_0)^{1/2}}, \tag{1}$$

where β is the beach slope, L_0 is the deep water wavelength given by linear theory and H_0 is the offshore wave height. Dissipative conditions are generally associated with low values of Iribarren parameters, typically less than 0.3 [*Stockdon et al.*, 2006; *Ruggiero et al.*, 2001; *Ruessink et al.*, 1998; *Raubenheimer and Guza*, 1996; *Raubenheimer et al.*, 1995; *Guza and Thornton*, 1982], whereas intermediate and reflective conditions are associated with larger values [*Holland and Holman*, 1999; *Holland*, 1995; *Holman*, 1986; *Holman and Sallenger*, 1985].

[4] The behavior of runup under dissipative conditions is different than during reflective and intermediate conditions. Combining *Miche*'s [1951] hypothesis and the analytical monochromatic, nonbreaking standing wave solution proposed by *Carrier and Greenspan* [1958], the normalized total vertical runup height S [*Guza et al.*, 1984; *Meyer and Taylor*, 1972; *Stoker*, 1947] becomes

$$\frac{S}{H_0} = \begin{cases} \left(\dfrac{\pi}{2\beta}\right)^{1/2} & : \xi_0 \geq \xi_c : \text{reflective} \\ \dfrac{\xi_0^2}{\pi} & : \xi_0 < \xi_c : \text{saturated} \end{cases}, \tag{2}$$

where $\xi_c = (\pi^3/2\beta)^{1/4}$. In the saturated region of equation (2), S is independent of the offshore wave height. Saturation experienced under dissipative conditions therefore implies that runup does not increase with increasing offshore wave height.

[5] Equation (2) applies to idealized conditions but does not account for the frequency distribution of runup on real beaches. Runup on natural beaches has been investigated by separating the infragravity S_{ig} (f < 0.05 Hz) and incident S_{inc} (f > 0.05 Hz) components. Indeed, runup heights within these bands are forced by different processes whose interplay changes depending on beach state. Using an extensive data set based on a variety of beaches and conditions, *Stockdon et al.* [2006] showed that on intermediate and reflective beaches, both frequency bands respond to increases in $(H_0L_0)^{1/2}$.

[1]EPOC, UMR 5805, University Bordeaux, OASU, CNRS, Talence, France.
[2]National Institute of Water and Atmosphere, Hamilton, New Zealand.
[3]Now at Environmental Hydraulics Institute, IH Cantabria, Universidad de Cantabria, Santander, Spain.
[4]Department of Earth and Ocean Sciences, University of Waikato, Hamilton, New Zealand.
[5]College of Oceanic and Atmospheric Sciences, Oregon State University, Corvallis, Oregon, USA.

0148-0227/11/2010JC006819

The same data set was used to show that while on dissipative beaches runup at incident frequencies, S_{inc}, saturates, runup at infragravity frequencies, S_{ig}, continues to grow with increasing $(H_0L_0)^{1/2}$. This finding was initially presented by *Guza and Thornton* [1982] who showed that S_{ig} varied linearly with H_0 (S_{ig} = 0.7 H_0). Similar findings have been presented by several other authors under dissipative [*Holman and Sallenger*, 1985] or even under highly dissipative [*Ruessink et al.*, 1998; *Ruggiero et al.*, 2004] conditions, although they did not agree on the value of the proportionality coefficient between S_{ig} and H_0.

[6] There is still a lack of understanding on the relation between infragravity runup height and environmental parameters. In particular, the role of the foreshore beach slope is still not well understood. Using a 90 min data set of 33 individual cross-shore transects spaced every 50 m in the alongshore, *Ruggiero et al.* [2004] reported that vertical infragravity runup elevation under high-energy dissipative conditions was linearly dependent on the local foreshore beach slope. Other studies [*Ruggiero et al.*, 2001; *Ruessink et al.*, 1998] showed instead that infragravity runup elevation on highly dissipative beaches could be scaled using offshore wave height alone. This result has been further supported by *Stockdon et al.* [2006] who also suggested that accounting for wave period allows for improved predictions of infragravity wave runup. Furthermore, attempts to link ξ_0 and S_{ig}/H_0 [*Ruessink et al.*, 1998; *Raubenheimer and Guza*, 1996; *Holland*, 1995; *Holman and Sallenger*, 1985] have failed to provide a consistent relationship to the point that *Raubenheimer and Guza* [1996] suggested this relationship could be site specific.

[7] Even though there was lack of evidence in the wide-ranging data set examined by *Stockdon et al.* [2006], there is increasing support for the hypothesis that during dissipative conditions, when infragravity energy dominates runup, the saturation commonly limiting S_{inc} also extends to infragravity frequencies [*Ruggiero et al.*, 2004; *Ruessink et al.*, 1998]. *Ruessink et al.* [1998] and *Ruggiero et al.* [2004] reported an f^{-3} and f^{-4}, respectively, spectral roll-off, typical of saturation, extending to frequencies in the infragravity band. The cause of infragravity saturation has been recently further investigated by several authors. *Battjes et al.* [2004] showed that the conventional gamma criterion used to distinguish breaking and nonbreaking incident waves on a slope also applied to infragravity waves near the shoreline, on the basis of which they postulated that the energy losses observed in their laboratory experiments were due to the breaking of infragravity waves. This was supported by further experiments by *van Dongeren et al.* [2004, 2007]. *Henderson and Bowen* [2002] indicated that the observed shoreline dissipation of infragravity waves might be due to the enhanced effect of bottom friction in very shallow water. However, *van Dongeren et al.* [2007] showed that the dissipation due to breaking was locally almost 20 times larger than the dissipation due to bottom friction and concluded that bottom friction was not the agent for infragravity wave energy dissipation. Similar conclusions had been reached analyzing field observations by *Henderson et al.* [2006] and *Thomson et al.* [2006] who suggested that energy was instead transferred from infragravity to incident wave frequencies. The wavefront steepening which caused infragravity breaking in the study of *van Dongeren et al.* [2007] was observed to be driven by energy transfer from infragravity to incident waves associated with self-self interactions of the infragravity waves in very shallow water.

[8] This work presents new data of runup elevation under conditions that have not been previously reported in the literature. While previous studies [*Ruessink et al.*, 1998; *Ruggiero et al.*, 2004] described highly dissipative conditions under gently sloping beaches (typically less than 0.03), the data presented here were collected during very high energy conditions associated with a 10 year return storm event, characterized by offshore wave heights of 6.4 m and peak period up to 16.4 s. Since the storm occurred during spring tide, the swash region experienced unusually steep foreshore beach slopes (higher than 0.05 and up to 0.08) while the surf zone was characterized by much milder slopes and was in a dissipative state. Aside from reporting detailed observations of runup under extreme offshore conditions, the objective of this work is to increase understanding of swash dynamics under extreme (because of the large offshore wave heights and wave periods) and peculiar (the cross-shore profile is constituted by a steep swash zone and a mildly sloping surf zone) conditions. By analyzing variations in infragravity and incident swash during the experiment, we aim to characterize swash saturation and in particular the hypothesis that also infragravity swash can show signatures of saturation (as suggested by *Ruessink et al.* [1998] and *Ruggiero et al.* [2004]). Finally, our data will also be used to test and extend to extreme values existing relationships [*Stockdon et al.*, 2006] for predicting runup elevation.

[9] The runup data obtained using video images are described in section 2, and results are presented in section 3. In section 4, we compare our results with previous studies linking infragravity runup to environmental conditions (mainly *Stockdon et al.* [2006], *Ruggiero et al.* [2004], and *Ruessink et al.* [1998]). Finally, conclusions are provided in section 5.

2. Methods

[10] Runup data were obtained during the ECORS-Truc Vert'08 beach experiment (France). The field experiment lasted 6 weeks, from 3 March to 13 April 2008. Truc Vert'08 was designed to measure beach modifications with emphasis on large winter waves, three-dimensional morphology, and macrotidal conditions. Hydrodynamic processes, sediment characteristics and transport, and morphodynamics of the beach were measured over many spatial and temporal scales and are summarized by *Senechal et al.* [2011].

[11] The field site (Figure 1) is situated on the southern part of the French Atlantic coastline (Figure 1, left) and is typical of the relatively natural coast extending 100 km between the Gironde Estuary (90 km to the north) and the Arcachon inlet (10 km to the south). This sandy coast is bordered by high aeolian foredunes (Figure 1, right). The sediment consists primarily of medium grained quartz sand with a median diameter of about 0.35 mm [*Lorin and Viguier*, 1987]. More recent work [*Gallagher et al.*, 2011] reported that mean surface grain size varies with the morphology, with coarser sediments (~0.6 mm) observed in the deeper rip channels and finer sediments (~0.3 mm) observed on the shoals between the rips. On the shoreface the mean grain size is nearly 0.35 mm. Truc Vert beach exhibits complex three-dimensional and highly dynamic morphologies commonly involving two distinct

Figure 1. Aerial view of Truc Vert beach at low tide. Notice the aerial image was not captured during the field experiment when no regular transverse bar pattern was present.

sandbar systems. The inner bar (see Figure 1, right) can experience all the states within the intermediate classification [see *Wright and Short*, 1984; *Masselink and Short*, 1993] and usually exhibits a Transverse Bar and Rip morphology [*Senechal et al.*, 2009]. The outer bar system exhibits long-term persistent crescentic patterns at a narrow range of wavelengths and the shape of which varies from symmetric to asymmetric [*Castelle et al.*, 2007]. During the present field experiment, the inner bar was nearly 2DH at the beginning of the storm and became slightly 3-D during the storm probably because of a Shoreward propagating accretionnary waves [see *Almar et al.*, 2010], while the outer bar became 2DH over the same period. No beach cusps were observed during the field experiment and the upper beachface was relatively uniform in the alongshore direction. The field site experiences an annual mean spring tidal range of 3.7 m. Alongshore tide-driven currents in the nearshore zone are essentially negligible. The wave climate is energetic with an annual mean significant wave height of 1.36 m and mean period around 8 s associated with long distance swells traveling mainly from NNW directions. The wave climate has a clear seasonal dependence with higher waves in winter than in summer (see *Butel et al.* [2002] for a complete wave classification of the Aquitanian coast).

[12] During the experiment, waves ranged from small swells (offshore significant heights, H_0, ranging from 0.3 to 2 m and peak periods, T_p, between 12 and 16 s) to heavy swells with a maximum H_0 of 8.1 m, on 10 March, associated with a peak period 16 s to 18 s (Figure 2). This event, a storm with a 10 year return period, coincided with large tidal amplitudes (more than 4 m, Figure 2), and was also characterized by a narrow-banded frequency and directional spectrum. As our

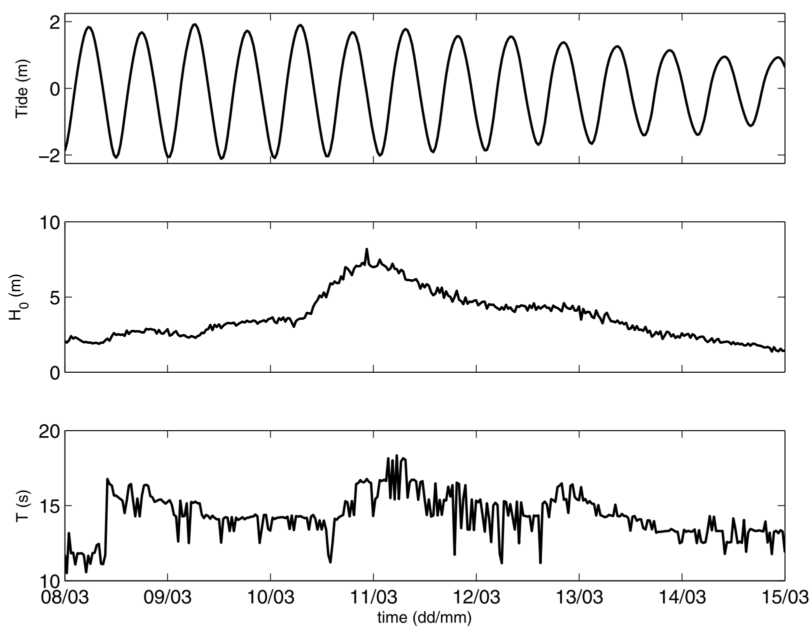

Figure 2. Hydrodynamic conditions during the experiment. (top) Theoretical tide (data provided by the French Navy), (middle) significant wave height and (bottom) peak period measured by a wave buoy in 20 m water depth are shown.

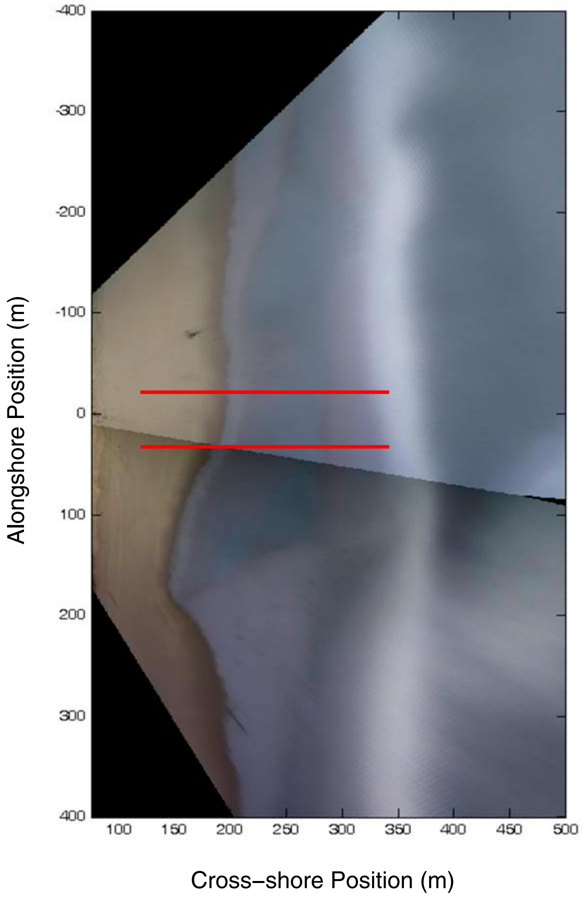

Figure 3. Plan view images from 10 min time-averaged video exposure of Truc Vert beach at high tide on 8 March 2010. The two solid lines indicate the position of the cross-shore transects used in this study.

main interest was in runup characteristics during extreme storm conditions, the data discussed in this paper will focus on this extreme event from its onset to the decay (8–15 March). Sea state conditions were measured with a directional Mark III Datawell waverider buoy anchored in 20 m depth situated offshore of the field area, about 1.5 km from the beachface.

[13] Throughout the experiment, runup was measured with a video system mounted on an 8 m high scaffolding built on the top of the dune backing the beach. The height of the camera above mean sea level was about 27 m. The system contained two high-resolution digital cameras (hereafter referred as North and South camera). Overlap in the field of view of the two cameras allowed for continuous coverage of the swash zone so that, overall, an alongshore distance of about approximately 600 m at high spring tide could be covered. The data discussed below consist of 89 fifteen min wave runup elevation time series measured along 2 individual cross-shore transects spaced by 50 m. The sampling frequency of the video system and of the derived runup time series was 2 Hz. One transect was obtained from camera South and the other one from camera North (Figure 3). The use of two transects each from a different camera was critical to cover the full duration of the event. Indeed during the apex of the storm, images from camera North were not used because of the wind and heavy rain facing the camera while camera South, pointing in a different direction, was less affected and provided data that could be used for analysis. On the other hand, images from camera South could not always be used because light during the sunset rendered the images unusable for analysis. Runup elevation time series were mostly acquired around high tide to maximize stationarity of the location of wave breaking and of the area of the foreshore over which runup propagated. During the apex of the storm, runup elevation time series were acquired during rising conditions because the high tide occurred at nighttime. The mean water level elevations for the time series considered in this study, according to in situ pressure measurements, varied by less than 0.4 m for each day.

[14] The runup along the selected transects (Figure 3) was manually digitized by two operators. Runup and rundown were identified as a white edge moving back and forth in the swash zone (Figures 4a–4c). To extract runup elevations along individual transects from video, the topography of the beach is needed in addition to the geometry of the cameras. To obtain the beach surface topography, a survey using Real Time Kinematic Differential Global Positioning System (RTK DGPS) was performed at each low tide (see *Parisot et al.* [2009] for a full description). Photogrammetric relationships [*Holland et al.*, 1997] were used to convert the digitized runup into time series of water level elevation relative to the French National datum (Figures 4d–4f). The vertical resolution of the runup elevation, depending both on lens properties and distance from the cameras, was estimated by mapping the horizontal pixel resolution (typically <1.0 m) to the elevation along the cross-shore transect. Despite the steep beach slope (see below and Table 1) the vertical resolution was less than 0.10 m for all the data analyzed in this work.

[15] Energy spectra, PSD (f), were computed from detrended, tapered data segments of 1800 points (900 s). The runup data were then partitioned to determine the incident band component (0.05 Hz < f < 0.24 Hz) and the infragravity band component (0.004 Hz < f < 0.05 Hz). Because of the large wave periods encountered during the peak of the storm, we have also repeated the analysis using a cutoff between infragravity and incident bands equal to 0.04 Hz and found that results reported in sections 3 and 4 show limited sensitivity to the choice of such frequency cutoff. Runup heights, S, were calculated as

$$S = 4^* \sqrt{\sum PSD(f)df}. \tag{3}$$

[16] Runup heights in the incident band, S_{inc}, and in the infragravity band, S_{ig}, were calculated by summing only over frequencies within the specified limits.

[17] Since the digitization of the rundown could be prone to subjectivity between the two operators, especially during extreme storm conditions, the accuracy of the digitizations was analyzed by comparing the transect runup heights obtained by the two operators from the same runs. Differences between runup height values from the two operators were always less than 10%.

[18] Finally, the definition of the foreshore beach slope β in this study was taken, in agreement with other studies of swash zone hydro- and morphodynamics [*Coco et al.*, 2004; *Ruggiero et al.*, 2004] to be the linear slope within the

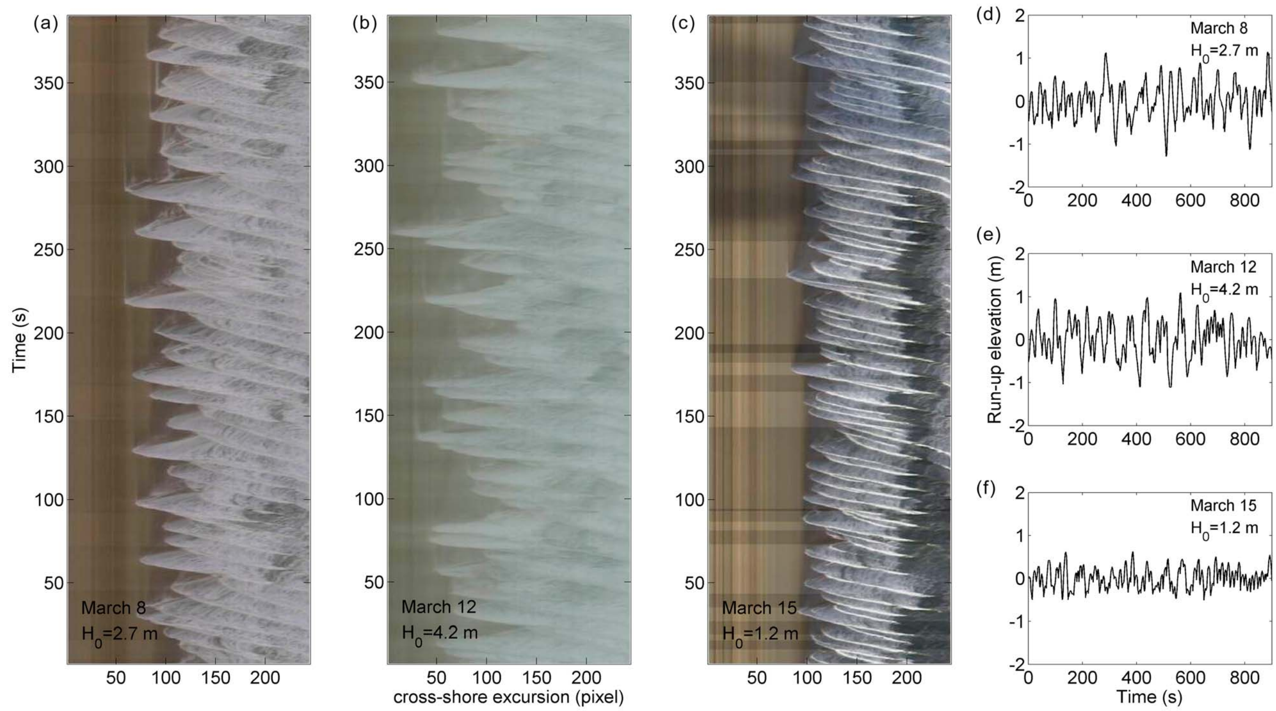

Figure 4. Example time stacks during (a) moderate (8 March), (b) energetic (12 March), and (c) calm conditions (15 March) and (d–f) detrended runup elevation time series.

region between ±2 standard deviations from the mean runup elevation.

3. Results

[19] An overview of environmental parameters is reported in Table A1 provided in Appendix A. Conditions during the period analyzed were very energetic with an associated mean offshore significant height of 2.5 m and maximum heights reaching up to 6.4 m (Table 1). The incident wave period was also very long with a mean of 11.2 s and maximum reaching 16.4 s (Table 1). Apart from data collected by *Ruggiero et al.* [2001] where wave periods equal to 17 s were measured, the values we report are substantially higher than the ones previously discussed in the literature under dissipative saturated conditions (see *Stockdon et al.* [2006] for a review). The average foreshore beach slope experienced during the storm was 0.06. The high spring tidal levels experienced during the experiment imply that the swash region is located landward of where the foreshore is characterized by increasingly steeper slopes due to the presence of embryonic dunes [*Capo et al.*, 2009]. Figure 5 illustrates the intertidal beach profile for each day of the period analyzed and for each cross-shore transect (blue is for camera South and red is for camera North). Onshore and offshore limits (mean ±2 standard deviations) of runup excursion for each day (high tide) and each cross-shore transect are indicated by a circle and square, respectively. The horizontal excursion of runup is relatively short (typically less than 50 m) because of the steep foreshore slopes.

[20] A consequence of the steep foreshore beach slopes is the relatively high Iribarren numbers experienced during this field experiment (Table 1). The mean Iribarren parameter for the data set is 0.65 with minimum and maximum values being 0.47 and 0.87, respectively. Despite the highly dissipative conditions experienced in the surf zone during the field experiment, the values of the Iribarren parameter in the swash fall in the category of moderately reflective conditions. Figure 6 shows averaged spectra during the rising, apex and falling stages of the storm. The associated degrees of freedom (dof) for averaged spectra computed during rising and falling conditions is 18. During the apex of the storm, the dof decreases to 12 since only one transect could be used. Consistent with spectra collected under energetic conditions [e.g., *Ruessink et al.*, 1998] no significant peak (at confidence level 0.95) was observed in the infragravity band even though most of the energy variance is concentrated well below the 0.05 cut-off. A summary of runup parameters, obtained from the individual spectra (equation (3)) is given in Table 2. Table 2 shows that the mean significant vertical runup elevation S during this period was 1.5 m. It varied by a factor of 3 over the data set, ranging from 0.8 m, under the less energetic conditions, to 2.5 m under extreme storm conditions. The mean infragravity component (1.3 m) was higher than the incident one (0.6 m) by a factor 2 and experienced higher variations. A summary of nondimensional swash parameters is given in Table 3. Table 3 shows that the vertical runup was dominated by infragravity waves during most runs with the ratio S_{ig}/S

Table 1. Summary of Environmental Parameters

	H_0 (m)	T_0 (s)	β	ξ_0
Mean	2.5	13.6	0.06	0.65
Standard deviation	1.3	1.6	0.01	0.09
Minimum	1.1	11.2	0.05	0.47
Maximum	6.4	16.4	0.08	0.87

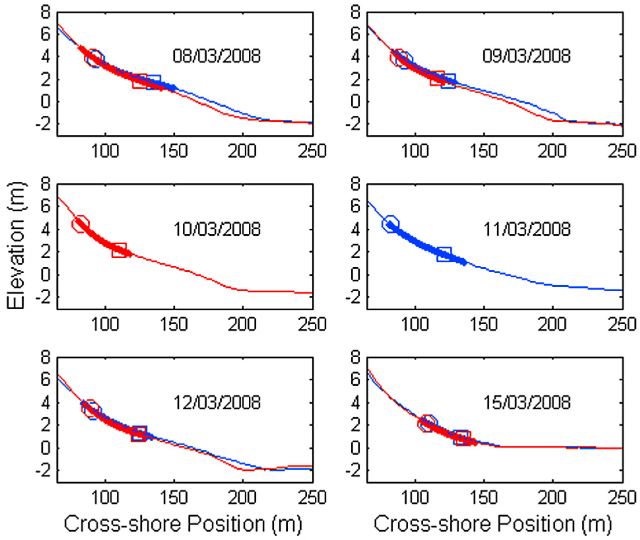

Figure 5. Cross-shore beach profiles corresponding to the positions where time stacks were collected. Blue is for camera south and red is for camera north. Onshore and offshore limits of runup excursion (mean ±2 standard deviations) for each day and each cross-shore transect are indicated by a circle and a square, respectively. Offshore is to the right. All time stacks were collected around high tide.

having an average value of 0.88, similar to the previous values reported in the literature under highly dissipative conditions [*Holman and Bowen*, 1984; *Ruessink et al.*, 1998; *Ruggiero et al.*, 2004; *Stockdon et al.*, 2006].

[21] In sections 3 and 4, empirical models based on regressions between the different parameters will be described. To evaluate these empirical models, the correlation coefficient

Table 2. Summary of Runup Parameters

	S (m)	S_{inc} (m)	S_{ig} (m)
Mean	1.5	0.6	1.3
Standard deviation	0.5	0.1	0.5
Minimum	0.8	0.4	0.6
Maximum	2.5	1.2	2.4

ρ and the 98% significant level, ρ_{sig}, are presented as a measure of the linear relationship between the two parameters. A summary of the regression coefficients, correlation coefficient (ρ), squared correlation (ρ^2) and RMS errors for all suggested parameterizations is presented in Table 4. As shown in Figure 7 (left), the total vertical runup elevation S (circles) is significantly correlated to H_0 (correlation coefficient ρ is 0.86, significant at the 0.02 confidence level). The slope of the best linear fit is 0.30 ± 0.05 and the intercept is equal to 0.73 (not shown in the figure). The presence of a high intercept (arising because of the saturated incident conditions) is somewhat counterintuitive as it implies a vertical runup of 0.73 m without waves. Forcing the fit linear line to intercept at 0 drastically decreases the coefficient correlation to 0.42 (still significant at the 0.02 confidence level). Despite the presence of some scatter in the data, Figure 7 shows that the vertical runup elevations are principally driven by the increase in S_{ig}. Variance in total vertical runup elevation represents only 5% of variance in offshore significant wave heights above 4.0 m whereas it represents 23% for offshore significant wave heights below 4 m. Variance in incident vertical runup elevation represents only 1% of variance in offshore significant wave height whereas variance in infragravity vertical runup elevation represents 12% of variance in offshore significant wave height. Saturation of the incident swash is even more evident when wave period is accounted for (Figure 8). Using a hyperbolic-tangent fit (S = 2.14 tanh(0.4H_0)) improves the correlation

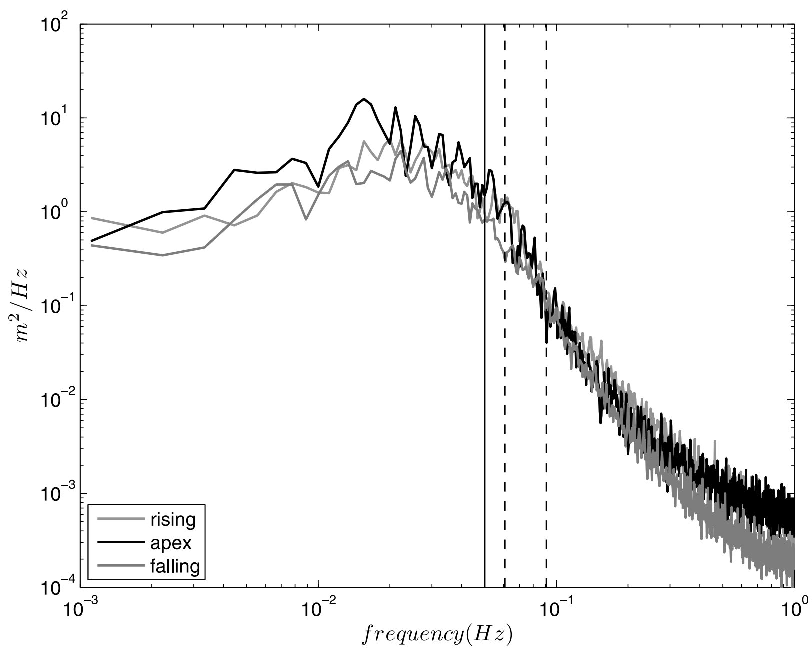

Figure 6. Averaged runup elevation spectra of the present data set during rising (dof = 18), apex (dof = 12), and falling (dof = 18) of the storm. The vertical solid line is the limit between the infragravity and incident bands (f = 0.05 Hz). The vertical dashed lines represent the concomitant offshore peak frequency.

Table 3. Overview of Nondimensional Runup Parameters

	S_{inc}/S	S_{ig}/S	S/H_0	S_{inc}/H_0	S_{ig}/H_0
Mean	0.42	0.88	0.66	0.28	0.58
Standard deviation	0.10	0.05	0.15	0.10	0.13
Minimum	0.22	0.75	0.31	0.11	0.27
Maximum	0.62	0.97	1.03	0.46	0.92

coefficient to 0.91 (Figure 7, left) which is a statistically significant improvement compared to the linear fit (at the 5% significance level, *F* test). The hyperbolic-tangent fit allows vertical runup to be 0 when the offshore significant wave height is 0 and also shows saturation to take place for values greater than 4.0 m as observed in the present data set.

[22] As shown in Figure 7 (right), the infragravity runup elevation S_{ig} is significantly correlated to H_0 (coefficient correlation is 0.84). The slope of the best linear fit is 0.29 ± 0.05 with an intercept equal to 0.59. This result closely agrees with *Ruggiero et al.* [2004] reporting $S_{ig} = 0.33H_0 + 0.33$. However, these results, in terms of both the slope and the intercept of the best fit, are higher than those predicted by *Ruessink et al.* [1998], $S_{ig} = 0.18H_0 + 0.16$. Again, the presence of a high intercept in our results is counterintuitive. Forcing the linear fit to a 0 intercept maintains statistically significant relationship and induces a slope of 0.48 ± 0.03, slightly smaller than the 0.7 found by *Guza and Thornton* [1982]. As the total runup *S* is dominated by the infragravity band, Figure 7 (right) also suggests S_{ig} to become saturated for offshore significant wave heights above 4. 0 m. The ratio of variance in infragravity vertical runup elevation over variance in offshore significant wave height decreases to 5% for offshore significant wave heights above 4 m (23% for offshore significant wave heights below 4 m). If one considers only the values obtained for offshore significant wave heights below 4.0 m, the slope of the best linear fit with an intercept forced to 0 is 0.62 ± 0.04, close to the value suggested by *Guza and Thornton* [1982] under similar offshore wave conditions. Using a hyperbolic-tangent fit improves the coefficient correlation to 0.90 (Figure 7, right). In particular, it allows infragravity component of vertical runup to be 0 when the offshore significant wave height is 0 and indicates saturation to take place for values greater than 4.0 m.

[23] Figure 9 illustrates the β dependence of both the infragravity S_{ig} and the incident S_{inc} components of runup. The solid line represents the regression proposed by *Ruggiero et al.* [2004] for foreshore beach slope below 0.05 and extended to the higher values of foreshore beach slope measured in the present data set. The Truc Vert data are consistent with the proposed regression by *Ruggiero et al.* [2004] for S_{inc}. The slope of the best fit linear line is 11.6 ± 4.7, consistent with the 11.4 slope established by *Ruggiero et al.* [2004]. The associated correlation coefficient is not too high (0.54) but is still statistically significant at the 0.02 confidence level. Our results also indicate that the linear correlation between the infragravity component S_{ig} and the foreshore beach slope is weakly (0.30) significant at the 0.02 confidence level, consistent with previous observations [*Ruggiero et al.*, 2004; *Ruessink et al.*, 1998].

[24] Figure 10 presents an overview of the relationships between ξ_0 and S_{ig}/H_0 published in the literature together with our observations. The Truc Vert data fall within a relative small intermediate range of Iribarren numbers ($0.5 < \xi_0 < 0.9$) and reveal a moderate, but significant at the 0.02 confidence level, dependence of normalized significant runup height on this parameter ($\rho = 0.53$). As previously mentioned, despite highly dissipative conditions in the surf zone, the range of Iribarren numbers in the swash zone falls within the intermediate and reflective conditions. The slope of the linear fit is 0.79 ± 0.33, slightly higher than the one proposed by *Ruggiero et al.* [2004] on a limited data set (only 9 points) when considering runup data with $\xi_0 > 0.3$ and much higher than the two other values previously proposed, 0.3 [*Holland*, 1995] and 0.53 [*Holman and Sallenger*, 1985]. On the other hand, it is much smaller than the 2.2 shown by *Ruessink et al.* [1998] and the 1.1 for $\xi_0 < 0.3$ proposed by *Ruggiero et al.* [2004]. As suggested by *Ruessink et al.* [1998], the use of a local parameter such as the Iribarren number may not be appropriate [see also *Herbers et al.*, 1995] especially for cases like the present one where the complexity of the beach profile (steep in the swash region and flat across the wide surf zone) cannot be reduced by a single beach slope parameter. It is also possible that the transition zone between dissipative and intermediate conditions is characterized by different relationships between S_{ig} and ξ_o. In line with the suggestion of *Ruessink et al.* [1998], we speculate that this transition zone strongly depends on the extent of saturation in the infragravity band as well as on the local mechanisms leading to energy dissipation (e.g., presence, location and depth of sandbars).

[25] Figure 11 represents the infragravity component Sig as a function of the dimensional parameter proposed by *Stockdon et al.* [2006]. Their extensive data set indicated

Table 4. Regression Parameters for Components of Runup Model

Quantity Modeled	Model Input	Slope (m)	Intercept b[a]	ρ (ρ_{sig})	ρ^2 (ρ^2_{sig})	RMSE (cm)
S	H_0	0.30 (±0.05)	0.73	0.86 (0.28)	0.74 (0.08)	23.7
S	H_0	0.53 (±0.04)	0	0.43 (0.28)	0.18 (0.08)	41.7
S	H_0	Hyperbolic Tangent		0.91 (0.28)	0.83 (0.08)	18.9
S_{ig}	H_0	0.29 (±0.05)	0.59	0.84 (0.28)	0.71 (0.08)	25.4
S_{ig}	H_0	0.48 (±0.03)	0	0.59 (0.28)	0.35 (0.08)	37.6
S_{ig}	H_0	Hyperbolic Tangent		0.90 (0.28)	0.80 (0.08)	20.5
S_{inc}	β	11.6 (±4.7)	−0.1	0.54 (0.28)	0.29 (0.08)	12.2
S_{ig}	β	20.8 (±17.1)	0.1	0.30 (0.28)	0.09 (0.08)	44.5
S_{ig}/H_0	ξ_0	0.79 (±0.33)	0.06	0.53 (0.28)	0.28 (0.08)	11.5
S_{ig}	$(H_0L_0)^{1/2}$	0.05 (±0.01)	0.10	0.91 (0.28)	0.83 (0.08)	19.1
S_{ig}	$(H_0L_0)^{1/2}$	Hyperbolic Tangent		0.91 (0.28)	0.83 (0.08)	18.8

[a]Intercept $b = 0$ indicates that regressions are forced through the origin.

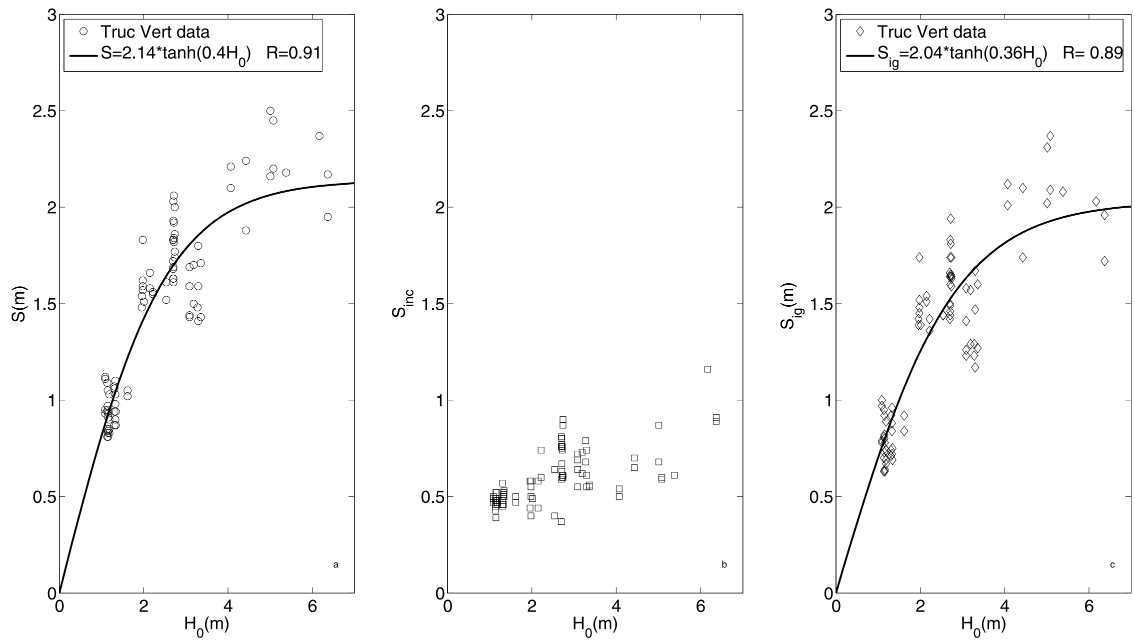

Figure 7. Vertical runup elevation versus offshore wave height H_0. (left) Total vertical runup elevation, (middle) incident component of vertical runup elevation, and (right) infragravity component of vertical runup elevation. Symbols represent observations, and line is the hyperbolic-tangent fit to observations.

that the magnitude of infragravity runup was linearly independent of the foreshore beach slope (consistent with our data set) and best parameterized as

$$S_{\mathrm{ig}} = 0.06(H_0 L_0)^{1/2}. \quad (4)$$

[26] Truc Vert data are consistent with the results provided by the large data set reported by *Stockdon et al.* [2006]. The correlation coefficient of the best linear line is relatively high (0.91) and the associated slope, 0.05 ± 0.01, is only slightly lower than the one reported by *Stockdon et al.* [2006]. This lower slope can be explained by the magnitude of infragravity runup S_{ig} associated to the highest $(H_0L_0)^{1/2}$ values that all fall below the predictor provided by *Stockdon et al.* [2006]. It is worth pointing out that these values (all characterized by $(H_0L_0)^{1/2}$ values higher than 35) are beyond the largest data reported by *Stockdon et al.* [2006]. Use of a hyperbolic-tangent fit provides a slight (statistically not significant) improvement to the linear fit but allows avoiding a non-physical intercept.

[27] To further analyze the possibility of saturation at infragravity frequencies, the infragravity band was subdivided into three classes, namely $0.004 < f < 0.025$ Hz, $0.025 < f < 0.035$ Hz, and $0.035 < f < 0.05$ Hz and the runup elevation was then determined for each class using equation (3). Results are shown in Figure 12. Runup elevations over the three frequency bands were about the same for H_0 less than 2 m, consistent with previous observations by *Ruessink et al.* [1998] who ascribed this to the white infragravity spectra under these conditions (see Figure 6, falling conditions). When the conditions become more energetic, $2 < H_0 < 3$ m, the runup elevation related to each frequency band tends to grow (more rapidly for the lowest-frequency band). If one considers only data for $H_0 < 3$ m, the slopes of the best linear fits are 0.45 ± 0.08, 0.30 ± 0.05, and 0.18 ± 0.05 for the lowest-frequency band, the middle-frequency band, and the highest-frequency band (correlation coefficients, respectively 0.88, 0.84 and 0.78 are all significant at the 0.02 confidence level), respectively. Beyond a value of the offshore wave height around 3–4 m runup elevation does not grow anymore for the highest-frequency band. With respect to the middle frequency band, we still observe a slight increase. The slope of the best linear fit is 0.13 ± 0.08 for $H_0 > 3$m (coefficient correlation is 0.67, significant at the 0.02 confidence level), that it is smaller than the value obtained for $H_0 < 3$ m. With respect to the lowest-frequency band, we also still observe a slight increase for offshore wave heights between 4 and 6 m although S_{ig} dis-

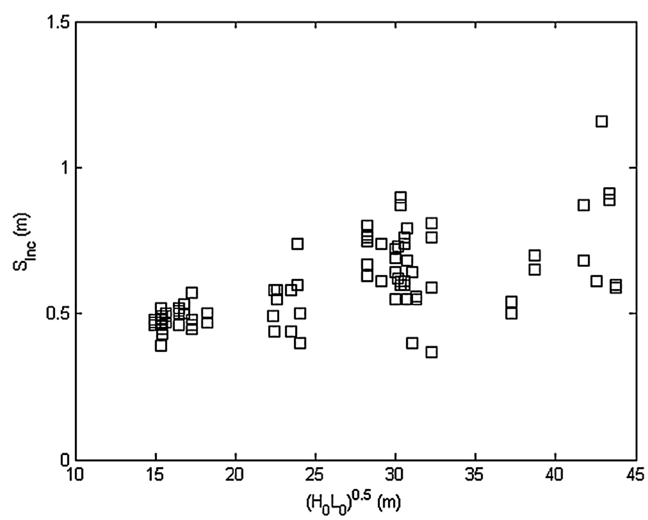

Figure 8. Incident, S_{inc}, runup as a function of $(H_0L_0)^{0.5}$.

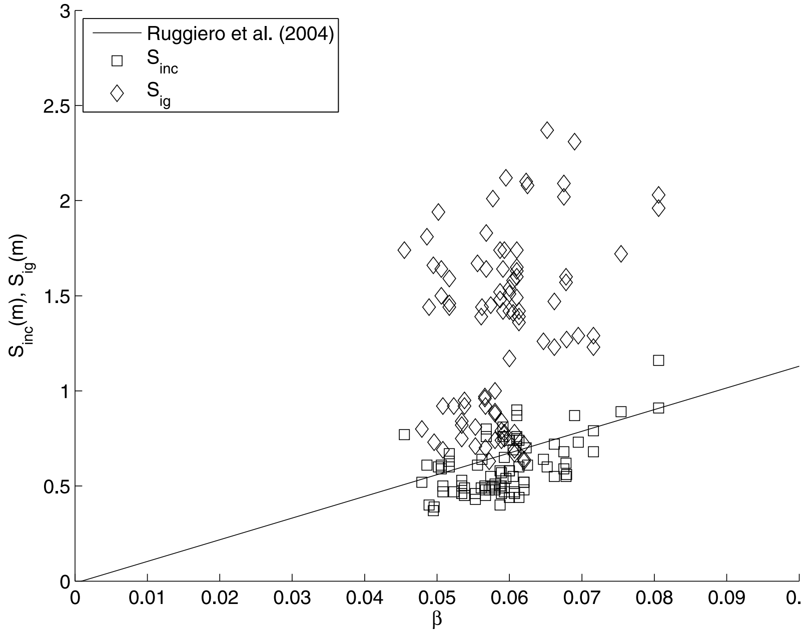

Figure 9. Incident and infragravity runup as a function of beach slope. Diamonds and squares refer to infragravity, S_{ig}, and incident, S_{inc}, runup, respectively. The solid line represents the extended linear relationship proposed by *Ruggiero et al.* [2004], $S_{inc} = 11.4\beta - 0.01$.

plays a noticeable decrease for the largest offshore wave heights.

4. Discussion

[28] We have presented new observations of wave runup during storm conditions. Time series of wave runup have been derived from video images of runup collected along two cross-shore transects from the onset to the decay of an extreme storm (10 year return period). To our knowledge, only three other works describing highly dissipative surf zone conditions are reported in the literature. *Holman and Bowen* [1984] presented results from runup records collected from 14 locations spaced irregularly over a 7 km

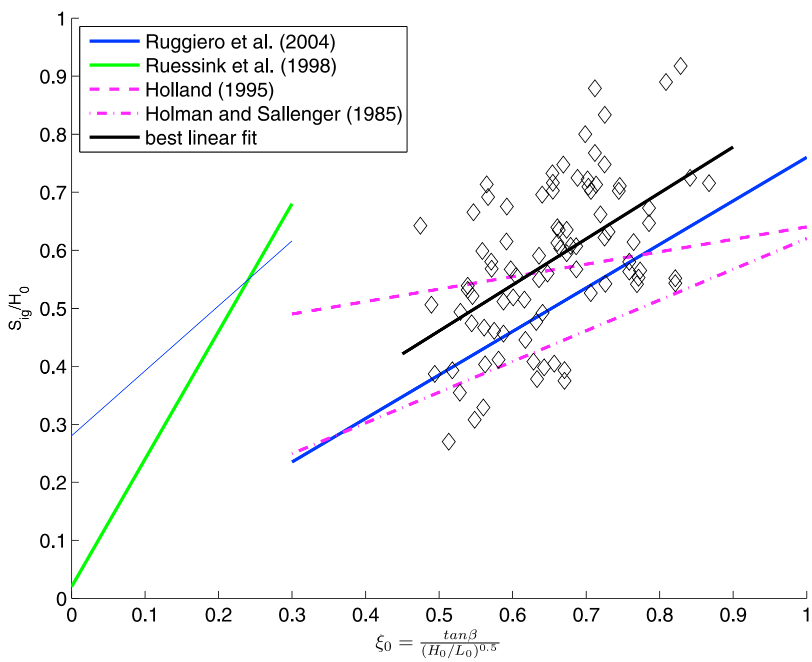

Figure 10. Overview of published relationships between ξ_0 and S_{ig}/H_0. The black symbols represent the present data set. *Ruggiero et al.* [2004] proposed two relationships for highly dissipative conditions ($\xi_0 <$ 0.3) and for moderate to reflective conditions ($\xi_0 > 0.3$).

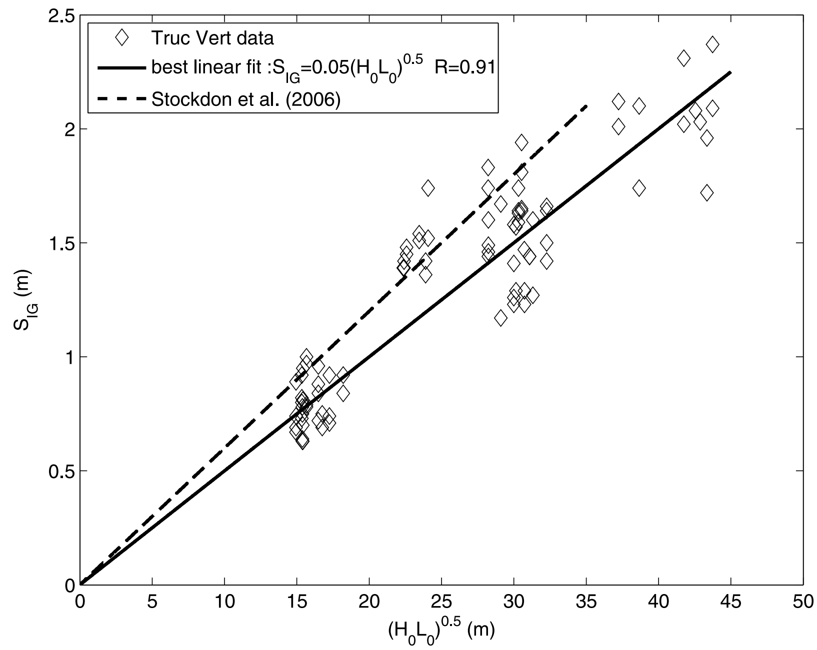

Figure 11. Infragravity runup elevation parameterized using the dimensional predictor proposed by *Stockdon et al.* [2006].

stretch of a low-slope beach in presence of significant wave heights up to 3.5 m with wave periods with a mean value of 15.5 s. *Ruessink et al.* [1998] presented results from a field experiment conducted in Terchelling (Netherlands). They experienced offshore significant wave heights up to 4.8 m with incident wave periods with a mean value of 10.7 s. The other work concerns data collected at Agate beach on the central Oregon coast [*Ruggiero et al.*, 2004]. Offshore wave height for such data set was 2.3 m and the incident wave period was 13 s. Despite highly dissipative surf zone conditions, these values are still low compared to the values experienced in the present study (Table 1). In particular, the Truc Vert data were collected during both high offshore significant wave heights (up to 6.4 m) and long periods (up

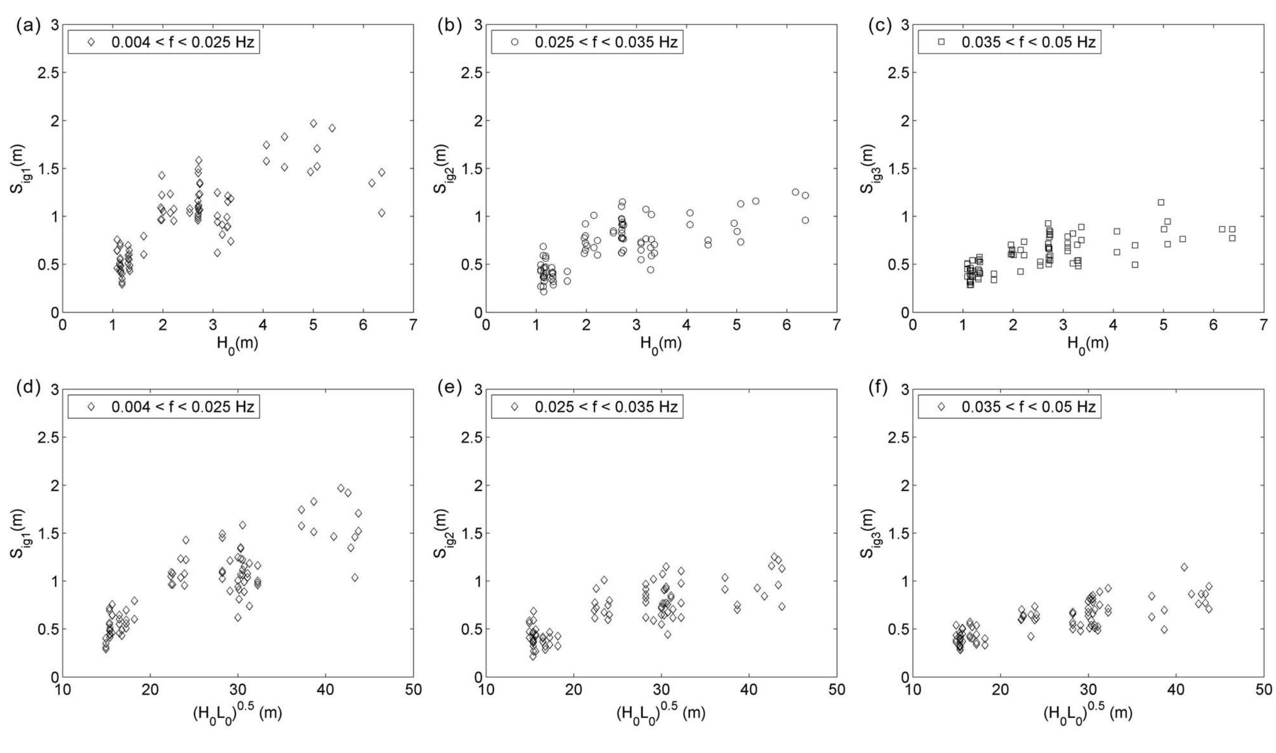

Figure 12. Runup elevations associated to different partitions of the infragravity band (a–c) versus offshore wave height H_0 and (d–f) versus $(H_0L_0)^{0.5}$.

to 16 s, see Appendix A for more details). The present data set is also novel due to these extreme wave conditions occurring with steep foreshore beach slopes β (Table 1). For example, the minimum foreshore slope experienced during our field experiment is higher than the maximum foreshore beach slope in the field experiments by both *Ruggiero et al.* [2004] and *Ruessink et al.* [1998]. Also, the associated mean foreshore beach slope is three times steeper than the mean slope examined by *Ruessink et al.* [1998] and *Ruggiero et al.* [2004]. The steep slopes characterizing the swash zone are in contrast with the mildly sloping surf zone. As a result of these peculiar conditions, the swash zone experiences nearly reflective conditions while the surf zone is in a dissipative state. The Iribarren number was developed for laboratory plane beaches, and its application to field studies has required a single beach slope value to characterize the whole cross-shore profile and, for the present conditions, this approach can be misleading.

[29] The total significant vertical runup elevation S varied by a factor of 3 over the data set, ranging from 0.81 m under the least energetic conditions to 2.50 m under extreme storm conditions (Table 2), and is correlated to H_0 (Figure 7), consistent with the previous observations. Nevertheless, Truc Vert runup values are higher than the ones reported by *Ruessink et al.* [1998] exposed to similar offshore significant wave heights. *Ruessink et al.* [1998] reported a maximum vertical runup elevation of 1.19 m associated with offshore significant waves of 4.8 m while Truc Vert data show a vertical runup elevation higher than 2 m for similar offshore significant wave heights. This difference can probably be ascribed to the associated wave period which was significantly higher in the Truc Vert data set, 15.4 s in the present case compared to 10.7 s as given by *Ruessink et al.* [1998]. If we compare the Truc Vert data to the ones reported by *Ruggiero et al.* [2004] who experienced similar periods and offshore significant wave heights, the difference in S is smaller but still present. In this case, the difference could be partly explained by the higher foreshore beach slope experienced in the Truc Vert data set. Indeed, various authors [*Stockdon et al.*, 2006; *Ruggiero et al.*, 2004; *Ruessink et al.*, 1998] found the significant vertical runup elevation to be linearly dependent on the local foreshore beach slope. Truc Vert data indicate a weak dependency of the incident vertical runup S_{inc} on foreshore beach slope (Figure 9). This weak dependency contrasts with the previous works under dissipative and lower-slope conditions [*Ruggiero et al.*, 2004; *Ruessink et al.*, 1998], where results indicated a high correlation coefficient. This is possibly related to both the limited range of β values (0.05–0.08) in the Truc Vert data set and to the combination of extremely energetic conditions and steep foreshore beach slopes.

[30] Truc Vert data support previous observations [*Ruggiero et al.*, 2001; *Ruessink et al.*, 1998] showing that runup on highly dissipative beaches can be scaled using offshore wave height alone (Figure 8). When using offshore wave height alone, the data suggests the possibility of runup saturation above approximately H_0 = 4m (Figure 7). This is also confirmed by further subdividing the infragravity frequency band into three classes (Figures 12a–12c). When conditions become more energetic, the growth in the runup elevation of the highest-frequency band is slower and nearly stops when H_0 exceeds a value of around 3.0 m. These observations are qualitatively consistent with previous observations [*Ruessink et al.*, 1998] showing that runup elevations in the $0.018 < f < 0.033$ Hz and the $0.033 < f < 0.05$ Hz frequency bands were arrested (i.e., full saturation) at a value around 3 m. The Truc Vert data also indicate that at the lowest-frequency band, $0.004 < f < 0.025$ Hz, saturation might take place when H_0 reaches a higher threshold (between 4.0 and 5.0 m). The data presented by *Ruessink et al.* [1998] did not support possible saturation of the very low frequency band and overall indicated a linear growth with increasing H_0, probably because of the less energetic conditions experienced in their data set. This result is intriguing and relevant (especially for those interested in the prediction of extreme runup) but should be taken with caution. The presence of an upper limit to wave runup and runup saturation also at infragravity frequencies should be studied on several other beaches before results can be generalized. Finally, the reason for the decrease in S_{ig} at the lowest-frequency band for H_0 > 6 m (Figure 12a) is unclear but it might be worth pointing out that the observations collected for the largest offshore wave heights (H_0 > 6 m) are not associated with the largest wave periods (see Appendix A). In fact, using a parameter that accounts for wave period, $(H_0L_0)^{1/2}$ (Figures 12d–12f), reduces the scatter and still shows saturation of the different infragravity bands. Scatter in the data distribution could be the result of the drastic morphological changes that occurred during the apex of the storm. In fact, video images showed the straightening of the outer bar and its migration 100 m offshore after about 1 day [*Almar et al.*, 2009, 2010]. The effect of crescentic bar horns, as well as the effect of bathymetric changes on runup (including changes from alongshore-variable to alongshore-uniform configurations), are expected to be small as the distance between the position of the timestacks and the closest onshore-protruding bar horn was about 150 m in the alongshore and around 500 m in the cross shore, at high tide. Although this an active area of research and 3-D bathymetric effects are unknown, it is worth reporting that for one beach of the Atlantic coast of the USA, *Stockdon et al.* [2006] found the bathymetry to have limited effect on runup predictability.

[31] Using $(H_0L_0)^{1/2}$ as a predictor of infragravity runup elevation results in a relationship extremely close to the predictor provided by *Stockdon et al.* [2006] and, importantly, collapses the data into a straight line (Figure 11). Overall, the $(H_0L_0)^{1/2}$ dependency further validates the findings of *Stockdon et al.* [2006] and indicates that the combination of wave period and height is critical in explaining variability of runup elevation. Appendix A shows in fact that the largest runup elevations are not necessarily associated with the largest offshore waves but they can also result from extremely large wave periods (and not extreme wave heights). Finally, consistent with *Stockdon et al.* [2006] the use of a predictor that includes beach slope does not improve the fit to the data (not shown).

5. Conclusions

[32] Observations of wave runup were collected during very high energy conditions characterized by offshore wave heights reaching up to 6.4 m and peak periods up to 16.4 s. At the same time, the swash region was characterized by relatively steep foreshore beach slopes (higher than 0.05 and

Table A1. Overview of Environmental Parameters

Run	H_0 (m)	T_0 (s)	H_0/L_0	α (deg)	β	ξ_0	S (m)	S_{inc} (m)	S_{ig} (m)
1	2.5	16.3	0.007	8	0.056	0.687	1.61	0.64	1.44
2	2.7	16.4	0.007	12	0.057	0.679	1.83	0.76	1.64
3	2.7	16.4	0.007	12	0.059	0.706	1.68	0.81	1.42
4	2.7	15.3	0.008	13	0.061	0.674	1.86	0.87	1.63
5	2.7	15.3	0.008	13	0.061	0.674	2.00	0.90	1.74
6	2.7	14.3	0.009	15	0.061	0.636	1.83	0.76	1.60
7	2.7	14.3	0.009	15	0.061	0.636	1.69	0.75	1.49
8	2.7	15.5	0.008	14	0.061	0.686	1.84	0.74	1.65
9	2.7	15.5	0.008	14	0.059	0.665	1.82	0.76	1.64
10	2.7	14.3	0.009	14	0.057	0.592	2.03	0.80	1.83
11	3.3	13.3	0.013	16	0.060	0.528	1.41	0.74	1.17
12	3.1	14.2	0.011	16	0.065	0.628	1.43	0.64	1.26
13	3.1	14.2	0.011	16	0.066	0.643	1.44	0.72	1.23
14	3.2	14.0	0.011	19	0.070	0.657	1.50	0.73	1.29
15	3.2	14.0	0.011	19	0.068	0.641	1.70	0.62	1.57
16	3.3	14.1	0.011	18	0.072	0.671	1.48	0.68	1.29
17	3.3	14.1	0.011	18	0.072	0.671	1.48	0.79	1.23
18	3.4	14.2	0.012	18	0.068	0.633	1.43	0.56	1.27
19	3.4	14.2	0.012	18	0.068	0.632	1.71	0.55	1.60
20	3.3	14.1	0.012	18	0.066	0.617	1.59	0.55	1.47
21	6.4	14.3	0.022	12	0.075	0.513	1.95	0.89	1.72
22	6.4	14.3	0.022	12	0.081	0.548	2.17	0.91	1.96
23	6.2	14.4	0.021	12	0.081	0.560	2.37	1.16	2.03
24	4.1	15.4	0.012	15	0.060	0.545	2.21	0.54	2.12
25	4.4	15.4	0.013	18	0.062	0.544	2.24	0.70	2.10
26	2.0	14.3	0.007	16	0.059	0.712	1.83	0.50	1.74
27	2.0	14.3	0.007	16	0.059	0.712	1.62	0.40	1.52
28	2.2	13.3	0.008	14	0.060	0.655	1.58	0.44	1.51
29	2.2	13.3	0.008	14	0.060	0.655	1.66	0.58	1.54
30	2.2	13.3	0.009	13	0.061	0.661	1.56	0.74	1.36
31	2.2	13.3	0.009	13	0.061	0.661	1.55	0.60	1.42
32	2.0	13.3	0.008	13	0.061	0.703	1.48	0.44	1.39
33	2.0	13.3	0.008	13	0.060	0.688	1.54	0.58	1.42
34	2.0	13.3	0.008	14	0.059	0.669	1.59	0.58	1.48
35	2.0	13.3	0.008	14	0.057	0.654	1.57	0.55	1.45
36	2.0	11.8	0.010	15	0.056	0.567	1.51	0.49	1.39
37	1.2	11.8	0.006	13	0.048	0.640	0.97	0.52	0.80
38	1.2	11.8	0.006	13	0.052	0.699	1.05	0.47	0.92
39	1.1	11.9	0.006	13	0.054	0.725	1.09	0.49	0.95
40	1.1	11.9	0.006	13	0.057	0.765	0.85	0.45	0.70
41	1.1	12.4	0.005	15	0.057	0.809	1.11	0.49	0.97
42	1.1	12.4	0.005	15	0.058	0.829	1.12	0.49	1.00
43	1.2	11.2	0.006	13	0.058	0.725	1.03	0.48	0.89
44	1.2	11.2	0.006	13	0.058	0.725	0.90	0.48	0.74
45	1.2	11.8	0.006	11	0.059	0.785	0.93	0.49	0.78
46	1.2	11.8	0.006	11	0.059	0.785	0.91	0.47	0.75
47	1.3	11.8	0.007	12	0.058	0.719	1.03	0.51	0.88
48	1.3	11.8	0.007	12	0.057	0.702	1.10	0.50	0.96
49	1.3	12.5	0.006	9	0.057	0.745	1.06	0.48	0.92
50	1.3	12.5	0.006	9	0.054	0.706	1.07	0.45	0.92
51	1.3	11.8	0.007	10	0.051	0.616	0.87	0.50	0.69
52	1.6	11.8	0.008	8	0.051	0.572	1.05	0.47	0.92
53	2.5	16.3	0.007	8	0.049	0.597	1.52	0.40	1.44
54	2.7	16.4	0.007	12	0.050	0.592	1.72	0.37	1.66
55	2.7	16.4	0.007	12	0.051	0.605	1.63	0.59	1.50
56	2.7	15.3	0.008	13	0.051	0.559	1.77	0.61	1.64
57	2.7	15.3	0.008	13	0.052	0.571	1.74	0.60	1.59
58	2.7	14.3	0.009	15	0.052	0.539	1.61	0.63	1.44
59	2.7	14.3	0.009	15	0.052	0.539	1.63	0.67	1.46
60	2.7	15.5	0.008	14	0.050	0.565	2.06	0.60	1.94
61	2.7	15.5	0.008	14	0.049	0.547	1.92	0.61	1.81
62	2.7	14.3	0.009	14	0.046	0.474	1.93	0.77	1.74
63	3.3	13.3	0.013	16	0.056	0.490	1.80	0.61	1.67
64	3.1	14.2	0.011	16	0.061	0.588	1.69	0.55	1.58
65	3.1	14.2	0.011	16	0.061	0.588	1.59	0.69	1.41
66	5.4	15.3	0.016	10	0.063	0.494	2.18	0.61	2.08
67	5.1	16.3	0.014	7	0.065	0.561	2.45	0.60	2.37
68	5.1	16.3	0.014	7	0.068	0.581	2.20	0.59	2.09
69	5.0	15.6	0.014	10	0.068	0.563	2.16	0.68	2.02
70	5.0	15.6	0.014	10	0.069	0.575	2.50	0.87	2.31
71	4.1	15.4	0.012	15	0.058	0.529	2.10	0.50	2.01
72	4.4	15.4	0.013	18	0.059	0.518	1.88	0.65	1.74
73	1.2	11.8	0.006	13	0.050	0.663	0.83	0.39	0.73
74	1.2	11.8	0.006	13	0.053	0.714	0.95	0.46	0.82
75	1.1	11.9	0.006	13	0.055	0.746	0.94	0.43	0.81
76	1.1	11.9	0.006	13	0.057	0.771	0.81	0.48	0.63
77	1.1	12.4	0.005	15	0.059	0.841	0.95	0.50	0.79
78	1.1	12.4	0.005	15	0.061	0.867	0.93	0.47	0.78
79	1.2	11.2	0.006	13	0.061	0.759	0.85	0.47	0.69
80	1.2	11.2	0.006	13	0.061	0.759	0.83	0.46	0.67
81	1.2	11.8	0.006	11	0.062	0.821	0.84	0.52	0.63
82	1.2	11.8	0.006	11	0.062	0.821	0.81	0.48	0.64
83	1.3	11.8	0.007	12	0.062	0.769	0.90	0.52	0.72
84	1.3	11.8	0.007	12	0.059	0.731	0.98	0.46	0.84
85	1.3	12.5	0.006	9	0.059	0.773	0.94	0.57	0.74
86	1.3	12.5	0.006	9	0.055	0.726	0.87	0.46	0.71
87	1.3	11.8	0.007	10	0.053	0.648	0.94	0.53	0.75
88	1.6	11.8	0.008	8	0.053	0.601	1.02	0.50	0.84

up to 0.08). This induced highly dissipative and saturated conditions over the low-sloping surf zone while the swash zone was associated with moderately reflective values of the Iribarren parameter (up to 0.87). The total significant vertical runup elevation S varied by a factor of 3 over the data set, ranging from 0.81 m, under the less energetic conditions, to 2.50 m at the peak of the storm. Our data show that the vertical runup elevations are driven by the increase in S_{ig} while the incident component S_{inc} is saturated, consistent with the previous observations reported in the literature under disspative conditions [*Stockdon et al.*, 2006; *Ruggiero et al.*, 2004; *Ruessink et al.*, 1998; *Holman and Sallenger*, 1985; *Guza and Thornton*, 1982]. Truc Vert data support the previous observations on highly dissipative beaches showing that runup can be scaled using offshore wave height alone but also extends the range of applicability of relations reported in the literature and indicates that accounting for wave period is critical in explaining runup variability. Our observations are consistent with previous laboratory [*van Dongeren et al.*, 2007] and field [*Ruggiero et al.*, 2004; *Ruessink et al.*, 1998] observations suggesting that saturation at infragravity frequencies is likely to occur. Furthermore, for extreme conditions, our observations indicate that saturation can dominate at almost all the infragravity frequencies. As a result, the best statistical predictor of runup is a hyperbolic-tangent fit showing saturation for extreme values of the offshore wave height. Although at present this result cannot be generalized to other beaches, the data presented in this contribution provides evidence of saturation at infragravity frequencies. Work is under way to assess the generality of these findings at other locations and the possible role of other variables (e.g., the effect of large-scale offshore morphology, angle of wave approach) on runup variability.

Appendix A

[33] Table A1 provides an overview of environmental parameters including offshore significant wave height (H_0), offshore wave period (T_0), wave incidence (α), foreshore beach slope (β), Iribarren number (ξ_0), runup heights (S), runup heights in the incident band (S_{inc}), and in the infragravity band (S_{ig}).

[34] **Acknowledgments.** We wish to thank all the organizations that have provided financial support for the field experiment, in particular the French DGA (ECORS project). This work was also done within the framework of BARBEC (ANR 2010 JCJC 602 01). Thanks also to Rafael Almar, George Payne, Vincent Marieu, and Antoine Réjas for the support in the installation of the video system; Jean-Paul Parisot, Sylvain Capo, and Stephan Bujan for the RTK DGPS data; and Jamie MacMahan for the in situ pressure measurements. G.C. is funded by the New Zealand Foundation for Research, Science and Technology; ISAT; and CNRS. Thanks to Bob Guza for stimulating this work. We would like to thank two anonymous reviewers for providing detailed reviews which have greatly improved the manuscript.

References

Almar, R., B. Castelle, B. G. Ruessink, N. Senechal, P. Bonneton, and V. Marieu (2009), High-frequency video observation of two nearby double barred beaches under high-energy wave forcing, *J. Coastal Res.*, *SI56*, 1706–1710.

Almar, R., B. Castelle, B. G. Ruessink, N. Senechal, P. Bonneton, and V. Marieu (2010), Two- and three-dimensional double-sandbar system behaviour under intense wave forcing and a meso-macro tidal range, *Cont. Shelf Res.*, *30*, 781–792, doi:10.1016/j.csr.2010.02.001.

Battjes, J. A. (1974), Surf similarity, paper presented at 14th Coastal Engineering Conference, Am. Soc. of Civ. Eng., Copenhagen.

Battjes, J. A., H. J. Bakkenes, T. T. Janssen, and A. R. Van Dongeren (2004), Shoaling of subharmonic gravity waves, *J. Geophys. Res.*, *109*, C02009, doi:10.1029/2003JC001863.

Butel, R., H. Dupuis, P. Bonneton, (2002), Spatial variability of wave conditions on the French Aquitanian coast using in-situ data, *J. Coastal Res.*, *SI36*, 96–108.

Capo, S., J. P. Parisot, S. Bujan, and N. Senechal (2009), Short time morphodynamic response of the Truc Vert beach to storm conditions, *J. Coastal Res.*, *SI56*, 1741–1745.

Carrier, G. G., and H. P. Greenspan (1958), Water waves of finite amplitude on a sloping beach, *J. Fluid Mech.*, *4*, 97–109, doi:10.1017/S0022112058000331.

Castelle, B., P. Bonneton, H. Dupuis, and N. Sénéchal (2007), Double bar beach dynamics on the high-energy meso-macrotidal French Aquitanian coast, *Mar. Geol.*, *254*, 216–223.

Coco, G., B. T. Werner, T. Burnet, and S. Elgar (2004), The role of tides in beach cusp formation, *J. Geophys. Res.*, *109*, C04011, doi:10.1029/2003JC002154.

Elfrink, B., and T. Baldock (2002), Hydrodynamics and sediment transport in the swash zone: A review and perspectives, *Coastal Eng.*, *45*, 149–167, doi:10.1016/S0378-3839(02)00032-7.

Gallagher, E. L., J. MacMahan, A. J. H. M. Reniers, J. Brown, and E. B. Thornton (2011), Grain size variability on a rip-channeled beach, *Mar. Geol.*, in press.

Guza, R. T., and E. B. Thornton (1982), Swash oscillations on a natural beach, *J. Geophys. Res.*, *87*, 483–491, doi:10.1029/JC087iC01p00483.

Guza, R. T., E. B. Thornton, and R. A. Holman (1984), Swash on steep and shallow beaches, paper presented at 19th Coastal Engineering Conference, Am. Soc. of Civ. Eng., Houston, Tex.

Henderson, S. M., and A. J. Bowen (2002), Observations of surf beat forcing and dissipation, *J. Geophys. Res.*, *107*(C11), 3193, doi:10.1029/2000JC000498.

Henderson, S. M., R. T. Guza, S. Elgar, T. H. C. Herbers, and A. J. Bowen (2006), Nonlinear generation and loss of infragravity wave energy, *J. Geophys. Res.*, *111*, C12007, doi:10.1029/2006JC003539.

Herbers, T. H. C., S. Elgar, R. T. Guza, and W. C. O'Reilly (1995), Infragravity-frequency (0.005–0.05 Hz) motions on the shelf, II, free waves, *J. Phys. Oceanogr.*, *25*, 1063–1079, doi:10.1175/1520-0485(1995)025<1063:IFHMOT>2.0.CO;2.

Holland, K. T. (1995), Foreshore dynamics: Swash motions and topographic interactions on natural beaches, Ph.D. thesis, Oreg. State Univ., Corvallis, Oreg.

Holland, K. T., and R. A. Holman (1999), Wavenumber-frequency structure of infragravity swash motions, *J. Geophys. Res.*, *104*, 13,479–13,488, doi:10.1029/1999JC900075.

Holland, K. T., R. A. Holman, T. C. Lippmann, J. Stanley, and N. Plant (1997), Practical use of video imagery in nearshore oceanographic field studies, *IEEE J. Oceanic Eng.*, *22*, 81–92, doi:10.1109/48.557542.

Holman, R. A. (1986), Extreme value statistics for wave run-up on a natural beach, *Coastal Eng.*, *9*, 527–544, doi:10.1016/0378-3839(86)90002-5.

Holman, R. A., and A. Bowen (1984), Longshore structure of infragravity wave motions, *J. Geophys. Res.*, *89*, 6446–6452, doi:10.1029/JC089iC04p06446.

Holman, R. A., and A. H. Sallenger (1985), Setup and swash on a natural beach, *J. Geophys. Res.*, *90*, 945–953, doi:10.1029/JC090iC01p00945.

Lorin, J., and J. Viguier (1987), Hydrosedimentary conditions and present evolution of Aquitaine coast, *Bull. Inst. Geol. Bassin Aquitaine*, *41*, 95–108.

Masselink, G., and M. G. Hughes (1998), Field investigation of sediment transport in the swash zone, *Cont. Shelf Res.*, *18*, 1179–1199, doi:10.1016/S0278-4343(98)00027-2.

Masselink, G., and A. D. Short (1993), The effect of tide range on beach morphodynamics and morphology: A conceptual beach model, *J. Coastal Res.*, *9*, 785–800.

Meyer, R. E., and A. D. Taylor (1972), Run-up on beaches, in *Wave on Beaches and Resulting Sediment Transport*, edited by R. E. Meyer, pp. 357–411, Academic, San Diego, Calif.

Miche, R. (1951), Le pouvoir réfléchissant des ouvrages maritimes exposés à l'action de la houle, *Ann. Ponts Chaussees*, *121*, 285–319.

Parisot, J. P., et al. (2009), Evolution of a multi-barred sandy beach in presence of very energetic events, *J. Coastal Res.*, *SI56*, 1786–1790.

Puleo, J. A., R. A. Beach, R. A. Holman, and J. S. Allen (2000), Swash zone sediment suspension and transport and the importance of bore-generated turbulence, *J. Geophys. Res.*, *105*, 17,021–17,044, doi:10.1029/2000JC900024.

Raubenheimer, B., and R. T. Guza (1996), Observations and predictions of run-up, *J. Geophys. Res.*, *101*, 25,575–25,587, doi:10.1029/96JC02432.

Raubenheimer, B., R. T. Guza, S. Elgar, and N. Kobayashi (1995), Swash on a gently sloping beach, *J. Geophys. Res.*, *100*, 8751–8760, doi:10.1029/95JC00232.

Ruessink, B. G., M. G. Kleinhans, and P. G. L. Van den Beukel (1998), Observations of swash under highly dissipative conditions, *J. Geophys. Res.*, *103*, 3111–3118, doi:10.1029/97JC02791.

Ruggiero, P., P. D. Komar, J. J. Marra, W. G. McDougal, and R. A. Beach (2001), Wave runup, extreme water levels and the erosion of properties backing beaches, *J. Coastal Res.*, *17*, 407–419.

Ruggiero, P., R. A. Holman, and R. A. Beach (2004), Wave run-up on a high-energy dissipative beach, *J. Geophys. Res.*, *109*, C06025, doi:10.1029/2003JC002160.

Senechal, N., T. Gouriou, B. Castelle, J. P. Parisot, S. Capo, S. Bujan, and H. Howa (2009), Morphodynamic response of a meso- to macro-tidal intermediate beach based on a long-term data set, *Geomorphology*, *107*, 263–274, doi:10.1016/j.geomorph.2008.12.016.

Senechal, N., et al. (2011), The ECORS-Truc Vert'08 nearshore field experiment: Presentation of a three-dimensional morphologic system in a macro-tidal environment during consecutive extreme storm conditions, *Ocean Dyn.*, in press.

Stockdon, H. F., R. A. Holman, P. A. Howd, and A. H. Sallenger Jr. (2006), Empirical parameterization of setup, swash and runup, *Coastal Eng.*, *53*, 573–588, doi:10.1016/j.coastaleng.2005.12.005.

Stoker, J. J. (1947), Surface waves in water of variable depth, *Q. Appl. Math.*, *5*, 1–54.

Thomson, J., S. Elgar, B. Raubenheimer, T. H. C. Herbers, and R. T. Guza (2006), Tidal modulation of infragravity waves via nonlinear energy losses in the surf zone, *Geophys. Res. Lett.*, *33*, L05601, doi:10.1029/2005GL025514.

van der Meer, J. W., and J. C. Stam (1992), Wave runup on smooth and rock slopes of coastal structures, *J. Waterw. Port Coastal Ocean Eng.*, *118*, 534–550, doi:10.1061/(ASCE)0733-950X(1992)118:5(534).

van Dongeren, A. R., J. Van Noorloos, K. Steenhauer, J. A. Battjes, T. T. Janssen, and A. Reniers (2004), Shoaling and shoreline dissipation of subharmonic gravity waves, in *Coastal Engineering 2004: Proceedings of the 29th International Conference*, edited by J. McKee Smith, pp. 1225–1237, World Sci., Hackensack, N. J.

van Dongeren, A. R., J. Battjes, T. T. Janssen, J. Van Noorloos, K. Steenhauer, G. Steenbergen, and A. Reniers (2007), Shoaling and shoreline dissipation of low-frequency waves, *J. Geophys. Res.*, *112*, C02011, doi:10.1029/2006JC003701.

Wright, L. D., and A. D. Short (1984), Morphodynamic variability of surf zones and beaches: A synthesis, *Mar. Geol.*, *56*, 93–118, doi:10.1016/0025-3227(84)90008-2.

K. R. Bryan, Department of Earth and Ocean Sciences, University of Waikato, Private Bag 3105, Hamilton 3240, New Zealand.

G. Coco, Environmental Hydraulics Institute, IH Cantabria, Universidad de Cantabria, Avda. de los Castros s/n, Santander E-39005, Spain.

R. A. Holman, College of Oceanic and Atmospheric Sciences, Oregon State University, 104 Ocean Administration Bldg., Corvallis, OR 97331, USA.

N. Senechal, EPOC, UMR 5805, University Bordeaux, OASU, CNRS, Avenue des Facultés, F-33405 Talence CEDEX, France. (n.senechal@epoc.u-bordeaux1.fr)